BIOCHEMISTRY
including biophysical chemistry & molecular biology

Article

pubs.acs.org/biochemistry

Comparative Molecular Dynamics Study of Human Islet Amyloid Polypeptide (IAPP) and Rat IAPP Oligomers

Guizhao Liang,[†,‡] Jun Zhao,[†] Xiang Yu,[†] and Jie Zheng*[,†]

[†]Department of Chemical and Biomolecular Engineering, The University of Akron, Akron, Ohio 44325, United States

[‡]Key Laboratory of Biorheological Science and Technology, Ministry of Education, Bioengineering College, Chongqing University, Chongqing 400044, P.R. China

ABSTRACT: Human islet amyloid polypeptide (hIAPP or amylin) is a causative agent in pancreatic amyloid deposits found in patients with type 2 diabetes. The aggregation of full-length $hIAPP_{1-37}$ into small oligomeric species is increasingly believed to be responsible for cell dysfunction and death. However, rat IAPP ($rIAPP_{1-37}$), which differs from hIAPP in only six of 37 residues, loses its aggregation ability to form toxic amyloid species. Atomic details of the effect of sequence on the structure and toxicity between the amyloidogenic, toxic hIAPP peptide and the nonamyloidogenic, nontoxic rIAPP peptide remain unclear. Here, we probe sequence-induced differences in structural stability, conformational dynamics, and driving forces between different hIAPP and rIAPP polymorphic forms from monomer to pentamer using molecular dynamics simulations. Simulations show that hIAPP forms from trimer to pentamer exhibit high structural stability with well-preserved in-register parallel β-sheet and the U-bend conformation. The hIAPP trimer appears to be a smallest minimal seed in solution. The stabilities of parallel hIAPP oligomers increase with the number of peptides. Conversely, replacement of hIAPP sequence by rIAPP sequence causes a significant loss of favorable interpeptide interactions in all rIAPP oligomers, destabilizing the C-terminal β-sheet, turn conformation, and overall stability. A less β-sheet-rich structure and a disturbed U-shaped topology exert a large energy penalty on the self-assemble of the rIAPP peptides into highly ordered, in-register β-sheet-rich protofibrils and fibrils, which explains the nonamyloidogenic activity of rIAPP. Moreover, the absence of interior water within the U-turn region in the well-packed higher-order hIAPP oligomers, not in the poorly packed rIAPP oligomers, also stabilizes peptide association. This work provides atomic details of the sequence−structure relationship between the amyloidogenic hIAPP and its analogues such as the nonamyloidogenic rIAPP and some mutants, which could help in the development of novel therapeutic agents to block the formation of toxic hIAPP oligomeric species for type 2 diabetes.

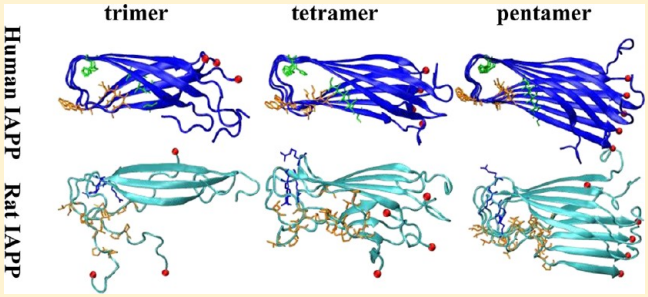

Human islet amyloid polypeptide (hIAPP or amylin), a 37-residue hormone peptide (KCNTATCATQ[10]RLANFL-VHSS[20]NNFGAILSST[30]NVGSNTY), is produced by pancreatic islet β-cells and cosecreted with insulin in response to glucose and other secretagogues.[1] The aggregation of hIAPP peptides into small soluble amyloid oligomers and large insoluble amyloid fibrils, which are deposited and found in the islets of Langerhans of more than 90% of type II diabetes patients, has been pathologically linked to the death of β-cells, the reduction of insulin production, and the action of insulin.[2] It is still unclear which of the hIAPP species, i.e., monomers, oligomers, protofibrils, or fibrils, induce toxicity to β-cells, but converging evidence has supported the "amyloid hypothesis" that small hIAPP oligomers are likely to be the most harmful species to β-cells, in common with other amyloidogenic oligomers formed by amyloid-β (Aβ) peptides associated with Alzheimer's disease[3] and α-synuclein peptides with Parkinson's disease.[4] The toxicity of hIAPP oligomers could be correlated with their interactions with the cell membrane. Such interactions are most likely to damage membrane integrity and functions, resulting in ionic homeostasis, oxidative injury, and altered signaling pathways.[5−9] Although the exact mechanisms of membrane damage induced by hIAPP oligomers remain controversial, a number of experimental and computational studies have led to several plausible mechanisms for membrane damage, including the formation of ion-permeable oligomeric pores, nonspecific binding of oligomers to cell membrane, or carpetlike membrane dissolution.[5,10−14] Because of a significant structural polymorphism of hIAPP oligomers, these different membrane disruption mechanisms appear not to be mutually exclusive.

The full-length $hIAPP_{1-37}$ peptide is composed of multiple function regions,[15] including an N-terminal region (residues 1−19) that involves membrane binding and insulin binding, a primary amyloidogenic region (residues 20−29), and a C-terminal region (residues 30−37) that involves peptide self-association. Fibrillar structures of full-length hIAPP have been

Received: November 11, 2012
Revised: January 15, 2013
Published: January 18, 2013

dx.doi.org/10.1021/bi301525e | *Biochemistry* 2013, 52, 1089−1100

extensively studied by atomic force microscopy, cryo-electron microscopy, solid-state nuclear magnetic resonance (NMR), and two-dimensional infrared (2D IR).[16−24] The hIAPP fibril structures consistently reveal that multiple U-shaped hIAPP monomers longitudinally stack on top of each other to form a parallel in-register β-sheet and each U-shaped hIAPP monomer consists of two antiparallel β-strands connected by a turn. Being more biologically relevant species, even hIAPP dimers can impair insulin secretion, resistance, and hyperglucagonemia,[25] but high-resolution atomic structures of hIAPP oligomers especially for small dimer to pentamer at the very early stage of amyloid aggregation are still lacking. In addition to their role as neurotoxic species, small oligomers could also serve as templated seeds for the growth of amyloid fibrils. The small size, transit nature, fast aggregation tendency, and heterogeneous conformations of hIAPP oligomers make it extremely difficult to capture and characterize their structural features via conventional experimental techniques.

A number of computational studies have provided some structural details for hIAPP monomer, oligomers, and template fibrils formed by full-length hIAPP or a fragment of the hIAPP peptide at the atomic level.[26−35] The full-length hIAPP monomers were found to exist as a rather large conformational variability, which could be attributed to the intrinsic flexibility of the hIAPP peptide and different computational conditions (i.e., force fields, solvation models, sampling algorithms, temperatures, and pHs). The hIAPP monomers could adopt a wide variety of conformations, including an unstructured coil,[34,35] a disordered conformation with transient α-helical structure,[26,28] a mixed α-helical and short antiparallel β-sheet,[35] a mixed helical and β-sheet structure,[34] an extended antiparallel β-hairpin,[35,36] and a compact helix−coil structure.[36] Similarly, experimental studies also show different and even controversial results for hIAPP monomers. A number of studies[19,37,38] reported that hIAPP monomers mainly adopted random structures using CD spectroscopy. Another CD study by Brender et al.[9] revealed that full-length hIAPP mainly adopted a random coil conformation at a low ionic strength of 25 μM and contained a small degree of β-sheet structure at a high ionic strength of 150 mM. However, Yonemoto et al.[39] and Williamson et al.[40] revealed the helical conformations with little β-sheet structure for hIAPP monomers using NMR. Even more complex conformations of hIAPP monomers were also characterized. Kayed et al.[23] described that the coexistence of two distinct conformers with both β-sheet and α-helix structural motifs. Dupuis et al.[36] combined ion mobility mass spectrometry and molecular dynamics (MD) simulations to investigate the structure of hIAPP monomers. They concluded that hIAPP monomers adopted two populated conformational families: an extended β-hairpin structure and a compact helix−coil structure.

For small hIAPP oligomers, Laghaei et al.[29] reported that a full-length hIAPP dimer displayed a strong expanded β-strand conformation between residues 17−27 and 29−35, which are required to form β-sheet for oligomerization. Dupuis et al.[30] found that hIAPP dimers form an extended β-hairpin conformation at residues 11−18 and 23−32 using combined ion mobility spectrometry−mass spectrometry and MD simulations. Barz and Urbanc[41] systematically compared the structure and dynamics of both Aβ_{1-40} and Aβ_{1-42} dimers and examined the effects of force fields of coarse-grained discrete MD and all-atom MD and water models of SPCE and TIP3P on resulting dimer structures. Simulations showed that dimer formation increased the level of structural disorder in Aβ_{1-42}, but not in Aβ_{1-40}, conformations. The structural difference between Aβ_{1-40} and Aβ_{1-42} dimers was not statistically significant using different water models and force fields. These computational studies have shown that hIAPP dimers have a larger conformational variability, and they also achieve a certain structural consensus with rich β-structure at residues 23−32. For other highly ordered hIAPP oligomers, MD simulations of the self-assembly process of multiple hIAPP$_{20-29}$[31,42,43] and hIAPP$_{22-27}$[44−46] peptides showed different slablike nuclei with different side chain packings at the interface, but the assembled β-sheets preferred to adopt antiparallel packing orientations with respect to each other. More interestingly, during the self-assembly process, the dewetting phenomenon was observed between adjacent β-sheets. In our recent study,[32,33] we have modeled and simulated a number of highly ordered hIAPP oligomers, which are generally classified into "stacking-sandwich" and "wrapping-cord" structures depending on β-sheet organization. In the stacking-sandwich structures, two or three β-layers are laterally stacked on top of each other in an antiparallel way to form a "sandwichlike" structure with either two-fold symmetry or asymmetry. The stacking β-layers are mainly associated by interdigitating overlapping side chains to form a steric zipper. Alternatively, multiple β-layers can wind around a hydrophobic core to form a "phone cord-like" structure with a certain periodicity. Unlike the stacking-sandwich models, the wrapping-cord structures can naturally accommodate the twist of cross-β-layers without causing severe structural defects, and therefore, they can accommodate more cross-β-layers to form a three-, four-, or five-fold fibril organization. Different stacking-sandwich and wrapping-cord hIAPP oligomeric structures serve as elementary templates for growth of fibrils via peptide elongation, reflecting a general and intrinsic nature of amyloid polymorphism. Similarly, Wang et al.[22] also proposed some structural models of two- and three-fold hIAPP protofilaments using 2D IR spectroscopy and MD simulations, compatible with our stacking-sandwich and wrapping-cord models.

More importantly, the rat and mouse IAPP sequence (rIAPP, KCNTATCATQ^{10}RLANFLVRSS^{20}NNLGPVLPPT^{30}NVGSNTY) differs from the hIAPP sequence in only six of 37 residues, but rats and mice do not develop diabetes-like symptoms even when rIAPP is overexpressed. Via six mutations (His18Arg, Phe23Leu, Ala25Pro, Ile26Val, Ser28Pro, and Ser29Pro) in hIAPP, six different residues of rIAPP are mainly located between residues 20 and 29, called a primary amyloidogenic region. Because of the high degree of sequence similarity and three hydrogen bond breakers of proline residues, rIAPP has been used as an inhibitor to prevent amyloid formation by hIAPP as previously demonstrated by thioflavin-T florescence, transmission electron microscopy, and circular dichroism.[47] There has been speculation that rIAPP can not aggregate into β-sheet-rich species,[48] which are required for amyloid toxicity. However, a striking finding recently showed that rIAPP peptides can also form their own amyloid β-sheet upon being templated with the hIAPP β-sheet rather than blocking the β-sheet formation of hIAPP.[49] Although the exact biological role of rIAPP serving as an inhibitor or a catalyzer to prevent or promote hIAPP β-sheet formation is still unclear, a number of studies have shown that cross-seeding of different but conformationally similar peptides may catalyze them to promote protein aggregation via conformational selection.[50−53] Thus, structure characterization of rIAPP peptides is critical for

Table 1. Summary of Simulation Systems with Structural Characteristics[a]

system	backbone root-mean-square deviation (Å)	R_g (Å)	normalized solvent accessible surface area (SASA)[b] (Å^2)	twist (deg)	time (ns), no. of runs
hIAPP1	16.3 ± 1.1	14.7 ± 0.8	4014.7 ± 173.4	–	50, 2
hIAPP2	7.4 ± 0.4	12.5 ± 0.2	2742.2 ± 116.3	27.0 ± 5.6	50, 2
hIAPP3	5.8 ± 0.2	14.7 ± 0.3	2322.1 ± 52.2	16.0 ± 1.6	50, 2
hIAPP4	5.3 ± 0.2	15.9 ± 0.2	2183.1 ± 50.3	12.8 ± 1.1	50, 2
hIAPP5	5.3 ± 0.3	16.5 ± 0.1	1957.1 ± 35.0	9.8 ± 0.9	50, 2
rIAPP1	11.1 ± 1.0	12.0 ± 0.5	3490.0 ± 140.9	–	50, 2
rIAPP2	10.8 ± 0.4	14.1 ± 0.3	2866.5 ± 92.6	32.9 ± 9.8	50, 2
rIAPP3	13.5 ± 0.3	17.9 ± 0.2	2808.9 ± 76.5	20.9 ± 1.2	50, 2
rIAPP4	9.1 ± 0.2	16.2 ± 0.1	2239.0 ± 54.5	13.4 ± 1.4	50, 2
rIAPP5	7.4 ± 0.3	17.9 ± 0.1	2144.5 ± 49.0	12.6 ± 1.0	50, 2

[a]All data are averaged from the last 10 ns simulations. [b]The total SASA values of hIAPP and rIAPP aggregates are normalized by the number of peptides for comparison.

a mechanistic understanding of hIAPP fibrillogenesis, toxicity, and inhibition, but major questions remain. What is the minimal size of the hIAPP seeds and their stability, and how sensitive is hIAPP oligomer formation to sequence changes? To better understand the structural features of and differences between the human and the rat versions of IAPP, we used the NMR-derived β-strand−turn−β-strand motif[17] as a building block to construct a series of hIAPP and rIAPP oligomers from dimer to pentamer with parallel peptide organization and to probe the differences in structural stability, conformational dynamics, and underlying stabilizing forces between hIAPP and rIAPP oligomers using all-atom MD simulations in explicit water. MD simulations show that the overall structural stability and β-sheet population of hIAPP oligomers significantly increase with the number of peptides. Small hIAPP oligomers such as trimer, tetramer, and pentamer are highly stable in the parallel organization at 330 K, suggesting that seeds for hIAPP aggregation can be quite small. Conversely, rIAPP oligomers from dimer to pentamer suffer from large secondary structure changes by losing β-strand conformation over time. Comparison of the structural stability of hIAPP and rIAPP oligomers reveals the importance of interpeptide hydrogen bonds in maintaining in-register peptide association. This work provides atomic details about hIAPP and rIAPP oligomeric structures, leading to a better understanding of the biological role of hIAPP oligomers in aggregation and toxicity mechanisms.

MATERIALS AND METHODS

hIAPP and rIAPP Models. Initial monomer coordinates of the $hIAPP_{1-37}$ peptide were extracted and averaged from 10 solid-state NMR-based structures as provided by the Tycko lab.[17] Each $hIAPP_{1-37}$ monomer had a β-strand−loop−β-strand (U-bend) fold consisting of two antiparallel β-strands connected by one turn [β-strand (Lys1−Val17)−turn (His18−Leu27)−β-strand (Ser28−Tyr37)]. An intramolecular disulfide bond between Cys2 and Cys7 was formed to stabilize the structure at the N-terminus. The N- and C-termini were blocked by NH_3^+ and COO^- groups, yielding a net charge of +3 at pH 7.4. An $hIAPP_{1-37}$ oligomer (from dimer to pentamer) was constructed by packing $hIAPP_{1-37}$ monomers on top of each other in a parallel and in-register manner, with an initial peptide−peptide separation distance of ∼4.7 Å, corresponding to the experimental data.[17] All starting structures of $rIAPP_{1-37}$ from monomer to pentamer were built from the corresponding $hIAPP_{1-37}$ structure by replacing side chains of six targeted residues (i.e., His18Arg, Phe23Leu, Ala25Pro, Ile26Val, Ser28Pro, and Ser29Pro), but without changing the backbone conformations and side chain orientations. The structures of the $rIAPP_{1-37}$ monomer and oligomers were first minimized for 1000 steps using the steepest decent algorithm with the backbone of the protein restrained before being subjected to the following MD simulations. All models are summarized in Table 1.

Explicit Solvent MD Simulation. All MD simulations were performed using NAMD[54] with the CHARMM27 force field for peptides and the modified TIP3P model for water.[55] Each oligomer was solvated in a TIP3P water box with a margin of at least 15 Å from any edge of the water box to any peptide atom. Each system was then neutralized by adding Cl^- and Na^+ ions to mimic an ionic strength of ∼200 mM. The resulting systems were subjected to 5000 steps of steepest decent minimization with peptide backbone atoms harmonically constrained, followed by 5000 additional steps of conjugate gradient minimization without any constraint. Short 1 ns MD simulations were performed to heat the system from 0 to 330 K by constraining the backbones of oligomers. The production MD simulations were performed using an isothermal−isochroic ensemble (*NPT*, where T = 330 K and P = 1 atm) under periodic boundary conditions. The Langevin piston method with a decay period of 100 fs and a damping time of 50 fs was used to maintain a constant pressure of 1 atm, while the Langevin thermostat method with a damping coefficient of 1 ps^{-1} was used to control the temperature at 330 K. The simulation temperature of 330 K is slightly higher than the physiological temperature of 310 K and helps to aid in avoiding kinetic traps, which allow us to probe the stabilities and dynamics of rIAPP and hIAPP peptides more quickly in the limited simulation time.[56,57] All covalent bonds involving hydrogen were constrained by the RATTLE method so that a 2 fs time step was used in the velocity Verlet integration. van der Waals (VDW) interactions were calculated by the switch function with a twin-range cutoff at 12 and 14 Å. Long-range electrostatic interactions were calculated using the force-shifted method with a 14 Å cutoff. Structures were saved every 2 ps for analysis. All analyses were performed using tools within CHARMM, VMD,[58] and code developed in house.

RESULTS AND DISCUSSION

Structural Stability of hIAPP and rIAPP Monomers. The hIAPP and rIAPP monomers are the smallest building blocks to self-assemble into highly ordered oligomers. Atomic-resolution structural information for both hIAPP and rIAPP

dx.doi.org/10.1021/bi301525e | Biochemistry 2013, 52, 1089−1100

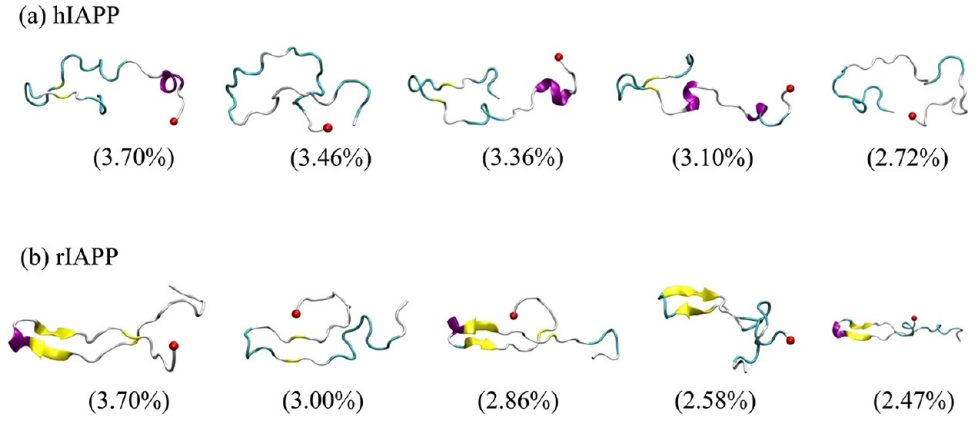

Figure 1. Five most populated representative conformations of (a) hIAPP monomer and (b) rIAPP monomer collected from a cluster analysis with a Cα rmsd cutoff of 5.0 Å. The population of each cluster is given in parentheses. The secondary structure is generated using the STRIDE program implemented in VMD. Color scheme for secondary structure: purple for α-helices, yellow for extended β-strand, cyan for turn, and white for random. The C-terminus of each conformation is shown as a red bead.

monomers can improve our understanding of the difference in the oligomerization mechanism between hIAPP and rIAPP peptides. Visual inspection of 50 ns MD trajectories clearly revealed that hIAPP monomer essentially lost its initial β-hairpin structure and folded into a mixed conformation of small β-strand at the C-terminus, random coil in the middle, and small α-helix at the N-terminus, leading to a large backbone root-mean-square deviation (rmsd) of 16.3 Å. We next clustered the similar conformations of hIAPP monomer using the cluster plugin in VMD with the criteria of a Cα rmsd cutoff of 5.0 Å. Figure 1a shows five representative conformations belonging to the five most populated clusters for hIAPP monomer. Each cluster represents a comparable structural population of ∼3.3%, representing a sum of ∼16.3% of all conformations. It can be seen that five representative hIAPP conformations displayed little transit β-strand and α-helical structures, but a large propensity for turn and random conformations, with values of 51.4 and 9.7%, 56.8 and 43.2%, 43.2 and 37.8%, 37.8 and 37.8%, and 43.2 and 56.8% in the five clustered conformations, respectively. This structural property is in reasonable agreement with experimental data that hIAPP monomer exists as a disordered structure in solution.[19,23,37,38] As described in the introductory section, all of these structural studies suggest that hIAPP monomers sample more complex and multiple conformations in solution. These different conformers not only equilibrate among random coil structure, partially helical structure, and β-hairpin structure but also dynamically balance with other highly ordered aggregates. No exact consensus about the secondary structure content of hIAPP monomers is achieved because of the complexity of hIAPP. It should also be noted that our conventional MD simulations have rather limited ability to search the large conformational space of monomers, and more populated monomeric structures could be obtained using highly efficient sampling techniques such as replica-exchange MD and Monte Carlo (MC) simulations.

Similar to hIAPP monomer, rIAPP monomer also lost its initial β-hairpin conformation and evolved into different clustered conformations with similar populations (Figure 1b). The percentages of turn and random conformations were 15.7 and 55.3%, 30.5 and 54.1%, 13.5 and 56.8%, 46.4 and 29.7%, and 35.1 and 40.5%, respectively, for the five representative clustered conformations. Reddy et al.[59] reported two populated conformations of rIAPP monomers in solution: one containing an α-helical conformation comprised of residues 7−17 and the other adopting a random coil conformation (in reasonable agreement with our results). Moreover, the bend motif, stabilized by intramolecular contacts among Gly24, Pro25, and Val26 and Leu16, Val17, and Arg18, was consistently presented in all five rIAPP clusters. It appears that rIAPP monomer displays a stronger tendency to maintain the bend conformation at positions 16−26 than hIAPP monomer. Overall, both monomeric hIAPP and rIAPP exhibit little β-propensity because of the lack of stabilizing interactions from adjacent peptides. This in turn suggests that the inherent propensity to form β-sheet-rich aggregates requires additional intermolecular peptide−peptide interactions. It should be noted that unlike replica-exchange MD or MC simulations, our conventional MD simulations sample an only relatively small conformational space, and thus, these representative hIAPP and rIAPP clusters are not necessarily excluded from other populated conformations.

Structural Stability of hIAPP and rIAPP Oligomers. The 37-residue hIAPP peptides can polymerize into different heterogeneous oligomers. Although these hIAPP oligomers are structurally diverse and transit, most of them contain β-sheet-rich structure, and some of them could act as seeds of nuclei for subsequent fibrillization. Figure 2 shows the final MD snapshots of hIAPP and rIAPP aggregates from monomer to pentamer at 330 K and neutral pH. For hIAPP systems, despite the dramatic decrease in rmsd values from monomer (16.3 Å) to dimer (7.4 Å) (Table 1 and Figure 3a), the parallel β-strands in hIAPP dimer, particularly C-terminal β-strands, were still largely disturbed, but two hIAPP peptides of the dimer still remain associated and retain a certain degree of extended β-strand structure. As the number of peptides continuously increased to the hIAPP trimer, tetramer, and pentamer, they displayed very high structural stability with comparable rmsd values of ∼5.3, 5.3, and 5.8 Å, respectively. The parallel in-register β-strands and the U-shaped peptide topology in trimer, tetramer, and pentamer were well maintained, with a typical twist of ∼4° between adjacent β-strands. The presence of a twist is consistent with experimental data obtained from NMR of hIAPP fibrils[17] and might represent a prerequisite for the incorporation of oligomers into fibrils. Consistently, hIAPP monomer and dimer had larger residue-based root-mean-square

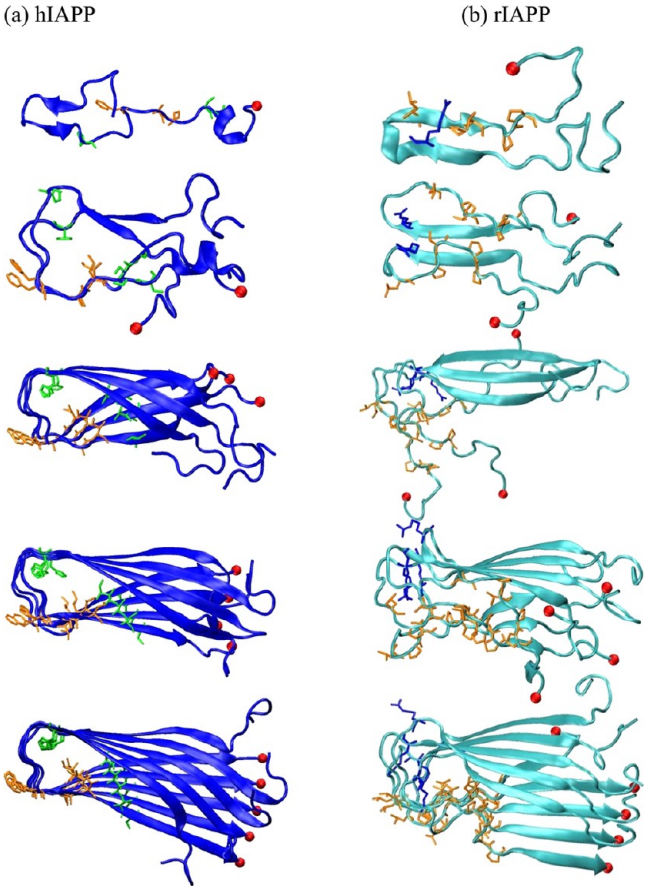

Figure 2. MD snapshots of (a) hIAPP (blue) and (b) rIAPP (cyan) aggregates from monomer to pentamer averaged from the last 10 ns simulations. Six residues at positions 18, 23, 25, 26, 28, and 29 are the locations of differences in sequence between hIAPP and rIAPP. Color scheme: green for polar residues, orange for nonpolar residues, and blue for negatively charged residues. C-Termini are shown as red beads for guiding the eyes, and water and ions were removed for the sake of clarity.

fluctuations (rmsf) than hIAPP trimer, tetramer, and pentamer across all residues (Figure 4a). It can be seen that the overall structural stability of hIAPP oligomers generally increases with the number of peptides. Although the hIAPP monomer and dimer exhibit rather larger conformational flexibility, addition of a single peptide from dimer to trimer dramatically enhances the structural integrity and β-sheet content of hIAPP aggregates, suggesting that small hIAPP trimer could act as a seed of nuclei for facilitating amyloid fibril formation and fibril growth. We also extended MD simulations of hIAPP trimer, tetramer, and pentamer to 80 ns. These oligomers still remained stable with well-organized parallel in-register β-sheets (data not shown).

It is important to quantify the role of amino acid sequence in the structure and dynamics of rIAPP aggregates from monomer to pentamer. At first glance, MD trajectories clearly showed that all rIAPP aggregates were structurally unstable, as also confirmed by large rmsd values of 11.1 Å for monomer, 10.8 Å for dimer, 13.5 Å for trimer, 9.1 Å for tetramer, and 7.4 Å for pentamer (Table 1 and Figure 3b). In contrast to the well-preserved β-sheets in hIAPP oligomers, the parallel, in-registere β-sheets were largely disrupted in rIAPP dimer to tetramer and less distorted in rIAPP pentamer. Figure 4b shows that the rIAPP tetramer and pentamer had very similar rmsf values, but the other rIAPP aggregates (i.e., monomer, dimer, and trimer) exhibited greater local fluctuations across all residues, especially for Arg18, Leu23, Pro25, Val26, Pro28, and Pro29. These six residues are located in the amyloidogenic region of residues 20−29, which plays an important role in fibril formation. As shown in Figure 2, the presence of these six residues in all rIAPP oligomers causes the turn and the C-terminal β-strands to be less stable than the N-terminal β-strands, resulting in the less populated β-conformation for residues 29−37 as compared to residues 1−17. We also performed additional 20 ns MD simulations for each hIAPP aggregate from monomer to pentamer at 310 K. MD trajectories showed that all rIAPP aggregates had unstable structures with disturbed turns at 310 K (data not shown), similar to these rIAPP oligomer structures at 330 K. The disturbed turn region in rIAPP tetramer and pentamer could prevent the rIAPP from stacking on top of each other to form high-order, in-register oligomers and fibrils. This preventative effect will become more pronounced as the peptide becomes elongated because of the unfavorable entropy effect. In addition, it is also possible that our preformed rIAPP oligomers could not resemble in vitro and in vivo aggregation of rIAPP; i.e., rIAPP may be not able to fold into the U-bent β-strand−turn−β-strand conformation or form β-sheet-rich seeds for fibril growth, and both effects would result in the prevention of the formation of rIAPP fibrils. The large structural instability of the rIAPP aggregates mainly arises from the loss of perfectly parallel packings from the C-terminal β-strands and the large movement of the turn regions.

In our previous study,[33] on the basis of NMR, mass per length, and electron microscopy, we have selected and determined three stable three-fold triangular hIAPP 15-mers (termed C-WT, N-WT, and T-WT) from a total of 72 triangular models by considering different packings among three U-shaped β-sheets. Although these three triangular hIAPP oligomers had different sizes, periodicities, sheet-to-sheet orientations and interfaces, and core-forming sequences at the cross section, all of them displayed high structural stability with

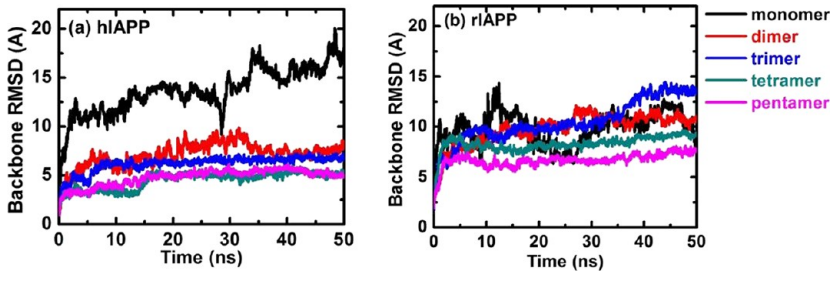

Figure 3. Backbone rmsds of (a) hIAPP and (b) rIAPP aggregates from monomer to pentamer with respect to their energy-minimized structures.

dx.doi.org/10.1021/bi301525e | *Biochemistry* 2013, 52, 1089−1100

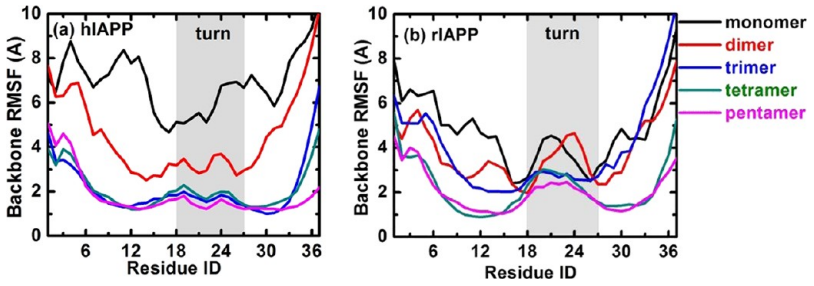

Figure 4. Residue-based backbone rmsf of (a) hIAPP and (b) rIAPP aggregates from monomer to pentamer with respect to their energy-minimized structures.

favorable layer−layer interactions. Upon introduction of the rIAPP sequence into three stable hIAPP structures via mutations (termed C-rat, N-rat, and T-rat), the N-rat and C-rat structures showed a strong tendency toward β-sheet disassociation. The T-rat structure was well maintained in the β-sheet association and the U-shaped topology comparable to that of the T-WT structure, but interactions between β-sheets were disfavored compared to those in the hIAPP T-WT model. Taken together, structural comparison of hIAPP oligomers with rIAPP oligomers suggests that because of the high structural stability and well-preserved U-shaped topology, hIAPP forms from trimer to pentamer could serve as seeds of nuclei to grow into fibrils via different growth pathways. For instance, they can longitudinally accommodate new monomers at the edges via the "lock-and-dock" mechanism[60] to form single-strand fibrils, laterally associate with other oligomers via stable C-terminal or N-terminal β-sheets to form multiple-strand sandwich-stacking fibrils, or incorporate more β-sheets via different fold symmetries to form multiple-strand wrapping-cord fibrils. Because of the defective U-shaped topology of the rIAPP oligomers, it is very unlikely that the rIAPP oligomers grow into the fibrils via three pathways as described above.

β-Sheet Population of hIAPP and rIAPP Oligomers. Many studies have shown that the formation of β-sheet structure is a general feature of the amyloid nucleus and fibrils.[21,61,62] Figure 5 shows the collective secondary structure of the hIAPP and rIAPP aggregates from monomer to pentamer as a function of time, while Figure 6 quantitatively measures the β-sheet population for all hIAPP and rIAPP aggregates using the DSSP algorithm.[63] The hIAPP monomer was unfolded into a disordered conformation containing a large population of coil, bend, and turn, and almost negligible β-structure (4.3%) near the turn region, suggesting that hIAPP monomer is not prone to the formation of significant β-structure alone in solution. For the hIAPP dimer, Figure 5 shows that the C-terminal β-strands largely lost their initial β-structure and were converted into an unstructured conformation, while the N-terminal β-strands (approximately three to five residues) retained a certain degree of β-structure. Although the overall U-shaped topology of the hIAPP dimer was still largely distorted, because of the increased level of interpeptide interactions, the β-sheet population was increased from 4.3% in monomer to 15.8% in dimer. Barz and Urbanc[41] recently reported that Aβ_{1-40} and Aβ_{1-42} dimers contained ∼15−25% β-structure, in good agreement with our β-structure propensity of 15.8%. Dupuis and co-workers[30] also reported that hIAPP peptides formed a β-strand-rich dimer. They proposed three different types of hIAPP dimerization, including side-by-side association of β-hairpin monomers, lateral stacking of β-hairpin monomers, and compact assembly of helical-coil monomers that convert into β-stand structure at the monomer−monomer interface. Our hIAPP dimer is in reasonably good agreement with the side-by-side β-hairpin association mode. Surprisingly, as hIAPP peptides continuously assembled into trimer or larger oligomers, the parallel in-register cross-β-structures were well preserved, and the β-sheet population dramatically increased to 49.2, 54.3, and 61.8% for the hIAPP trimer, tetramer, and pentamer, respectively (Figure 6).

A secondary structure content analysis of the rIAPP peptides revealed that the β-sheet content was maintained at 12.1% for monomer and 12.3% for dimer and then monotonically increased to 23.8% for tetramer, 26.6% for pentamer, and 38.2% for pentamer (Figure 6), showing an increased level of β-sheet structure as a function of the rIAPP polymorphic form, which is similar to the pattern for hIAPP oligomers. Particularly for the rIAPP forms from trimer to pentamer, the C-terminal residues that have sequences different from that of hIAPP suffered from a significant reduction in the level of β-sheet, whereas the N-terminal residues retained their initial β-strand conformation. The turn conformation also underwent large fluctuations during the entire simulations (Figure 7). This less β-sheet-rich structure and disturbed U-shaped topology exert a large energy penalty for the self-assembly of the rIAPP peptides into highly ordered, in-register β-sheet-rich protofibrils and fibrils, which explains the nonamyloidogenic activity of rIAPP.

Interpeptide Interactions Play an Important Role in Maintaining β-Strand Association. It is generally accepted that hydrogen bonding interactions between peptides are inherent to β-sheet stability. The number of hydrogen bonds between adjacent i and i + 1 peptides was calculated and normalized by the number of adjacent peptide pairs, n − 1, where n is the number of peptides, to allow direct comparison for different polymorphic forms of hIAPP and rIAPP peptides (Figure 8a). Comparing the β-sheet content in Figure 6 with the number of hydrogen bonds in Figure 8a revealed a clear correlation that regardless of sequence difference, the β-sheet content increased with the number of hydrogen bonds. For the stable hIAPP oligomers (i.e., trimer to pentamer), native hydrogen bonds between adjacent peptides were almost evenly distributed along two β-strand directions throughout the simulations. Once formed, these hydrogen bonds were rarely broken and acted as a zipper to retain the parallel in-register interchain organization. In contrast, the great loss of hydrogen bonds between adjacent peptides was observed for all rIAPP oligomers at the very early stage of simulations (∼10 ns). It can be seen in Figure 8a that as compared to that of each corresponding hIAPP oligomer, the number of hydrogen bonds was largely reduced by 50.0, 36.6, 28.1, and 26.9% for rIAPP dimer, trimer, tetramer, and pentamer, respectively. Proline is known to be a β-sheet breaker. The replacement of Ala25,

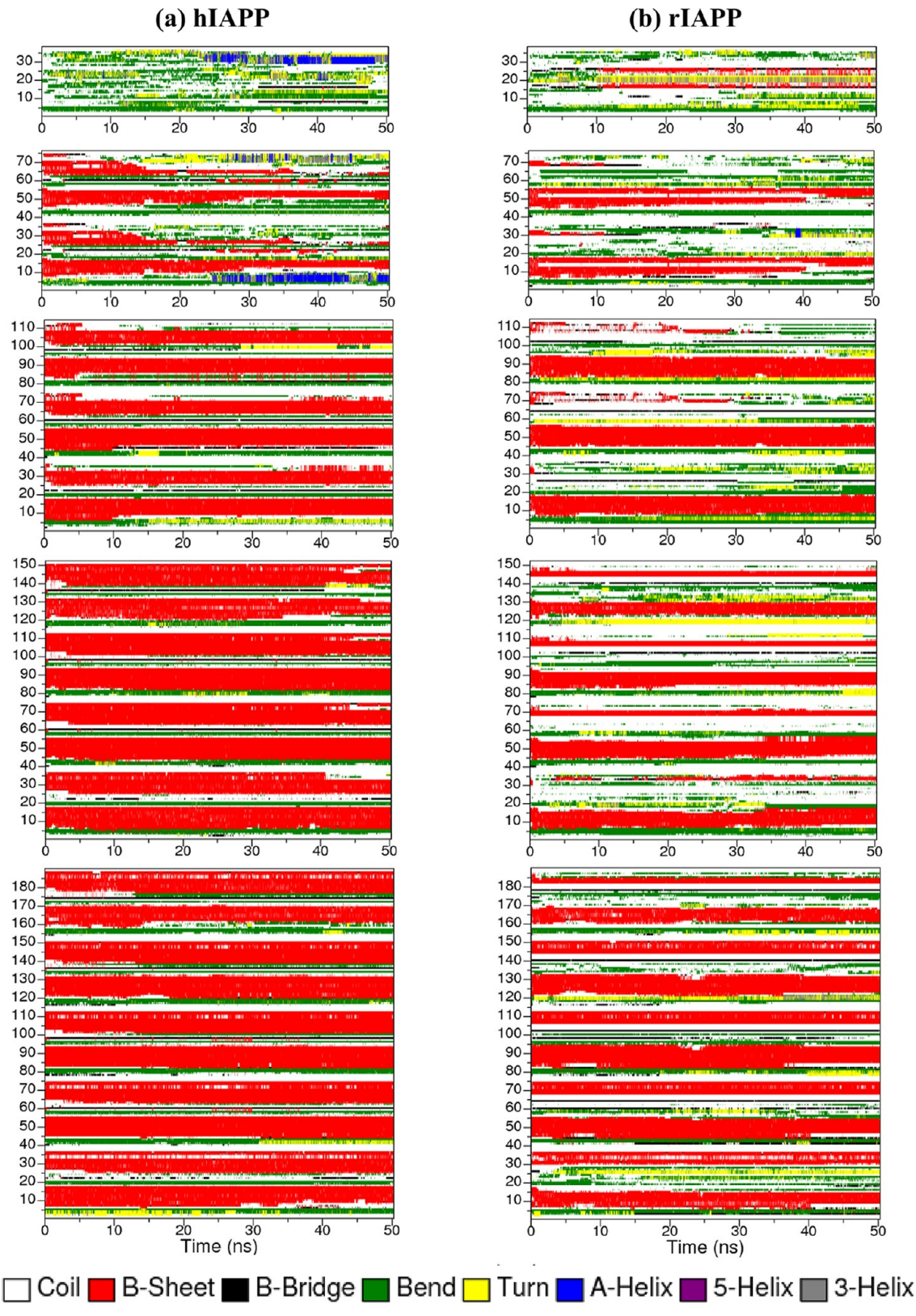

Figure 5. Secondary structure of (a) hIAPP and (b) rIAPP aggregates from monomer (top) to pentamer (bottom), as calculated by the DSSP algorithm.[63]

Ser28, and Ser29 in the hIAPP sequence with three prolines in the C-terminal β-strand region in the rIAPP sequence caused a loss of intermolecular hydrogen bonds between adjacent peptides and intramolecular contacts with its counterpart of the N-terminal β-strands, leading to a distorted β-sheet structure. Because the formation of hydrogen bonds requires strong distance and angular dependencies, hydrogen bonding interactions help not only in retaining the existing interchain

dx.doi.org/10.1021/bi301525e | *Biochemistry* 2013, 52, 1089−1100

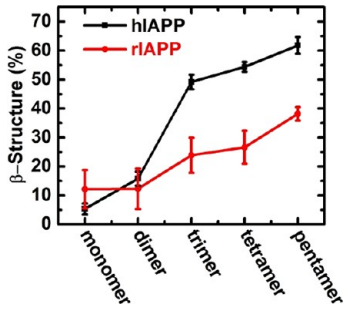

Figure 6. Averaged β-sheet content of hIAPP and rIAPP aggregates.

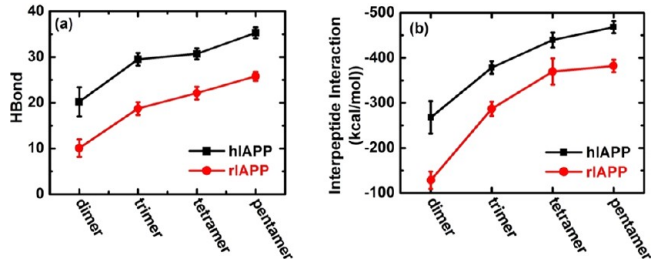

Figure 8. (a) Number of hydrogen bonds and (b) averaged interaction energy between any single peptide and other peptides in a given oligomer. There is a reasonable correlation between β-sheet content (Figure 6) and the number of hydrogen bonds and interpeptide interactions between peptides.

organization but also in reorganizing disordered peptide packings into a directional and ordered interchain arrangement.

In addition to hydrogen bonds, other interpeptide interactions such as hydrophobic interactions, $\pi-\pi$ stacking, and other side chain contacts can also contribute to the stabilization of β-sheet structure. To provide a more complete identification of driving forces underlying β-strand association, we calculated interpeptide interactions to explain the correlation between the overall structural stability and underlying peptide−peptide interactions. Because different oligomers have different numbers of peptides, to consider the effect of the size of oligomers on interpeptide interactions and to consistently correlate the interpeptide interactions with the overall structural stability of oligomers, we calculated the average interaction between any single peptide and other peptides in a given oligomer using the relationship $E_{\text{peptide-peptide}} = \sum_{i=1}^{n}\sum_{j>i}^{n} E_{ij}/n$, where i and j represent the ith and jth peptides in a given oligomer, respectively. In Figure 8b, the interpeptide interactions were normalized by the number of peptides (n) for direct comparison. The interpeptide interaction energies were −267.8, −378.6, −439.7, and −468.1 kcal/mol for hIAPP dimer, trimer, tetramer, and pentamer, respectively, while these interaction energies were reduced to −128.4, −286.8, −369.8, and −382.2 kcal/mol for rIAPP dimer, trimer, tetramer, and pentamer, respectively (Figure 8b). Clearly, a change in the sequence from hIAPP to rIAPP caused the loss of interpeptide interactions for each oligomer. Small hIAPP oligomers are more energetically favorable than rIAPP oligomers, suggesting that the hIAPP peptides are more likely to remain stable in solution for further peptide aggregation. Decomposition of interpeptide interaction energies into VDW and electrostatic contributions revealed that regardless of peptide sequence and size, VDW interactions (44.9−50.8%) were comparable to electrostatic interactions (49.2−55.1%), suggesting peptide association is in a cooperative mode. Moreover, the number of favorable interpeptide interactions decreased the most from dimer to trimer by 110.8 kcal/mol for hIAPP peptides and by 158.4 kcal/mol for rIAPP peptides, but the increasing trend was gradually slowed as the number of peptides decreased. This fact further supports the idea that hIAPP trimer could be serve as as seeds of nuclei for fibril formation and growth. Given an ideal separation distance of 4.7 Å between adjacent peptides and long-range interaction cutoff of 14 Å, it is reasonable to extrapolate that interpeptide interactions will eventually achieve a stable plateau for highly ordered oligomers (i.e., ≥7-mer). As expected, interpeptide interactions were well correlated with β-sheet content; i.e., the peptides have strong intermolecular interactions with their neighboring peptides, producing a well-ordered β-sheet structure with more stable and saturated hydrogen bonds between peptides. Thus, the structural stability and β-sheet content of hIAPP and rIAPP oligomers are more

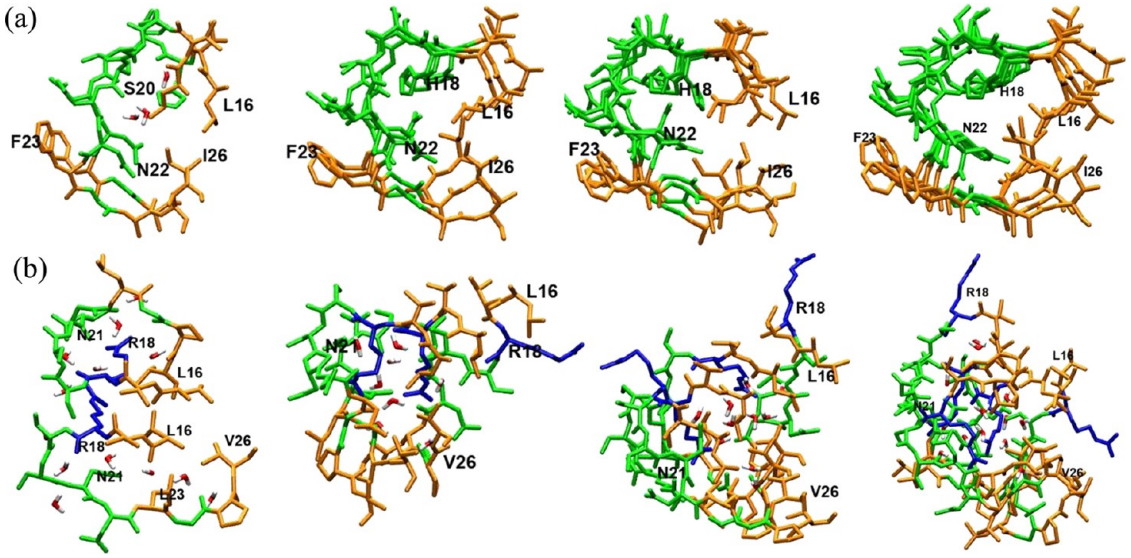

Figure 7. Conformations and internal hydrations of the turn regions (residues 16−26) of (a) hIAPP and (b) rIAPP oligomers from dimer (leftmost) to pentamer (rightmost). Some structurally important residues are labeled.

dx.doi.org/10.1021/bi301525e | *Biochemistry* 2013, 52, 1089−1100

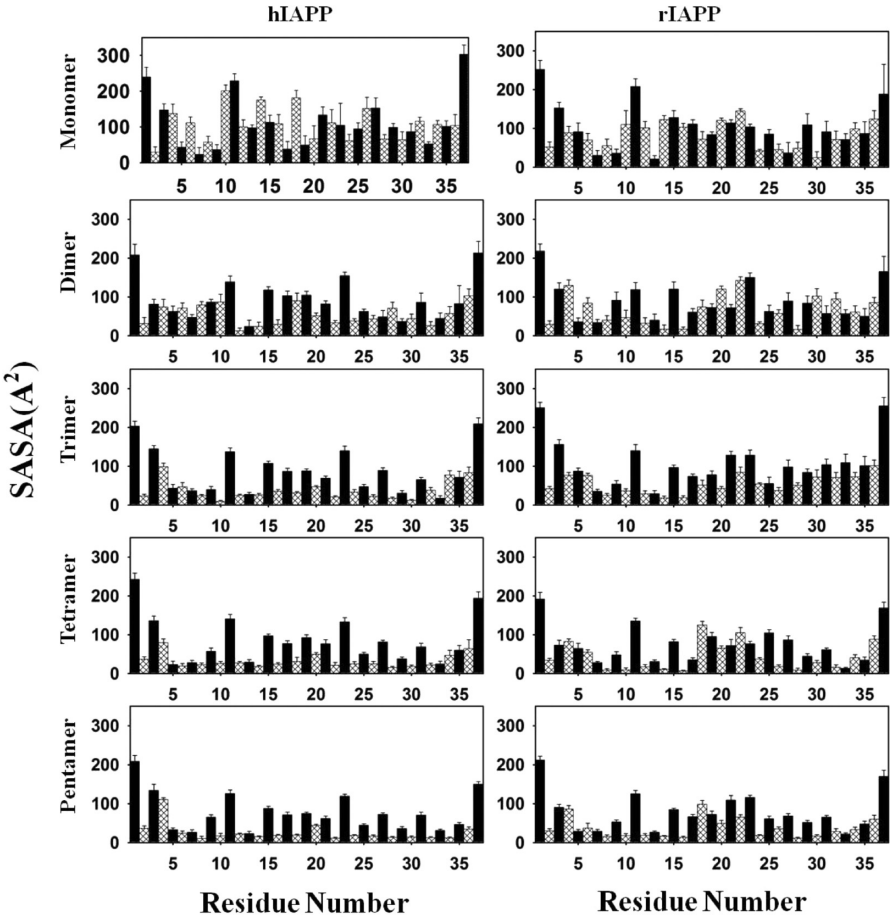

Figure 9. Solvent accessible surface area (SASA) of individual residues in hIAPP and rIAPP aggregates from monomer to pentamer. All data were averaged using structures from the last 10 ns of each simulation.

precisely attributed to a strong network of interactions between peptides. There was speculation that the formation of amyloid oligomers usually can be divided into two steps. The monomers rapidly collapse into disordered assemblies driven by strong interactions between hydrophobic residues, followed by the slow structural reorganization to characteristic β-structure driven by main chain hydrogen bonds.[64]

Hydration of hIAPP and rIAPP Oligomers. Water plays a significant role in mediating the structure and kinetics of early prefibrillar oligomers and final mature fibrils at different assembly stages.[65] The solvent accessible surface area (SASA) of hIAPP and rIAPP aggregates, normalized by the number of peptides, was calculated to quantify the hydration for each residue and each oligomer (Figure 9 and Table 1). Table 1 shows that, on average, regardless of hIAPP and rIAPP aggregates, the SASA values generally decreased with the number of peptides, with more dramatic decreases from monomer to dimer. As the size of peptide aggregates increased, more residues were well protected from solvent because of the formation of a well-ordered β-sheet structure. Similarly, because of the high structural stability, stable hIAPP oligomers exhibited relatively smaller SASAs than corresponding unstable rIAPP oligomers. A large SASA suggests not only the more exposed residues but also the larger dewetting barrier upon association with other peptides. In Figure 9, the SASA of each residue for both hIAPP and rIAPP aggregates was inhomogeneous, suggesting that residues have various ways of being exposed to water. For the oligomers with a relatively ordered β-sheet structure, residues pointing outward to bulk water (black bars) generally had larger SASA values than inward-pointing residues (dashed bars).

When hIAPP or rIAPP peptides pack in parallel along the fibril axis, they possess internal cavities formed by consecutive U-turns. The initial size of these internal U-turn cavities was ~4 Å, which is slightly large to accommodate water molecules inside. It is thus of interest to explore the structure and dynamics of confined water in the U-turn cavity in all hIAPP and rIAPP aggregates. The inspection of MD trajectories did not reveal interior hydration within the U-turn cavity in hIAPP forms from trimer to pentamer (Figure 7a). In those well-preserved U-turn cavities, compact inward-pointing side chain packing prevented water molecules from penetrating into the U-turn region, although the turn region consists of five consecutive hydrophilic residues (Hse18, Ser19, Ser20, Asn21, and Asn22). SASA data also indicated that the interior cavity of each stable U-turn formed by His18–Leu27 residues was almost solvent inaccessible for hIAPP forms from trimer to pentamer. We also extended MD simulations of hIAPP oligomers to 80 ns, but no internal hydration was observed for stable hIAPP oligomers from trimer to pentamer because of the highly integrated and compact turn conformation. Because of the relatively disordered and expanded turn conformation in hIAPP dimer, few water molecules can access and interact with turn residues. In contrast, the stronger internal hydration propensity observed for rIAPP was mainly due to the specific solvation of the disturbed turn region. All rIAPP oligomers

dx.doi.org/10.1021/bi301525e | *Biochemistry* 2013, 52, 1089–1100

displayed a disturbed turn conformation (Figure 7b), and the expanded interpeptide distances near the turn region allow water molecules to enter into and be trapped in the turn region during the simulations. Interior water would further destabilize intermolecular interactions between rIAPP peptides. It is apparent that a number of water molecules were confined between peptides to form certain hydrogen bonds with peptides.

Figure 10 shows the radial distribution function, $g(r)$, of the oxygen atoms of water (O_w) around the β-carbon atoms (C_B)

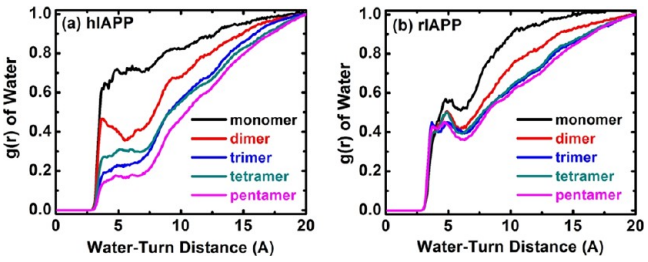

Figure 10. Radial distribution function, $g(r)$, of water molecules around the β-carbon (C_B) atoms of six inward-pointing turn residues at positions 16, 18, 20, 22, 24, and 26 for (a) hIAPP and (b) rIAPP polymorphic aggregates.

of six inward-pointing turn residues at positions 16, 18, 20, 22, 24, and 26. The height of $g(r)$ represents local water density (bulk water density of 1 g/cm^3). From all five $g(r)$ profiles in the hIAPP systems, the change in height of the $g(r)$ revealed the following decreasing order of the level of hydration near the turn region: monomer > dimer > trimer > tetramer > pentamer (reflecting the reduction of water molecules in the solvation shells near the turn region). The number of water molecules decreased >57% in the first solvation shell from the monomer system to the trimer, tetramer, and pentamer systems. Because of the dry condition inside the turn region (except for the dimer), no obvious hydration shells [i.e., peaks of $g(r)$] were observed at 3.5−7.5 Å for all systems, consistent with SASA and MD trajectories. On the other hand, $g(r)$ profiles of the rIAPP systems, particularly from trimer to pentamer, displayed almost identical water distributions (Figure 10b), in which the first hydration shell appeared at ∼5 Å with a local water density similar to 40−50% of bulk water density, suggesting that water molecules are able to access the disturbed turn region. The dramatic difference in water $g(r)$ profiles between rIAPP and hIAPP oligomers further confirms that the well-preserved turn cavity in the hIAPP forms from trimer to pentamer is likely to prevent water molecules from penetrating into the cavity because of the limited interior space and restricted side chain movement. It appears that the well-ordered and stable oligomers are less solvated than the disordered aggregates, and this evidentially suggests that desovaltion in hIAPP oligomers provides an additional favorable entropic contribution for facilitating the peptide aggregation process.

It is interesting to note that unlike the dehydrated U-turn cavity in hIAPP oligomers, the internal hydrated U-turn cavity was observed in Aβ oligomers,[57,66,67] which adopt β-strand−turn−β-strand motifs similar to those of hIAPP oligomers. The U-turn cavity in Aβ oligomers (6−7 Å) is larger than the U-turn cavity in hIAPP oligomers (4 Å), which may explain penetration of water molecules into the U-turn cavity. Meanwhile, confined water molecules stabilized interior Asp23−Lys28 salt bridges but were not trapped into a 4.8 Å space between neighboring peptides, which would otherwise induce destabilization. Additionally, Buchete et al.[68] reported that as finite Aβ oligomers grow into infinite Aβ fibrils, the desolvation of the U-turn cavity occurs. Despite the large energy and entropic penalty, desolvation is generally required to facilitate peptide assembly longitudinally and laterally, which forms different dry interfaces between in-register peptides and between multiple protofilaments.[69,70]

CONCLUSIONS

We have performed all-atom explicit solvent MD simulations to investigate the structural stability and dynamics of hIAPP and rIAPP aggregates from monomer to pentamer. All hIAPP and rIAPP oligomers are modeled by longitudinally stacking U-shaped peptides together to form an initial in-register parallel β-sheet. MD results show that hIAPP monomer and dimer are unstable in solution, but an increase in the level of order of peptides even from monomer to dimer can significantly enhance peptide association by increasing the number of favorable interpeptide interactions (enthalpy) and decreasing the level of intrapeptide conformation change (entropy). This becomes even more pronounced for higher-order oligomers. Small hIAPP oligomers such as trimer, tetramer, and pentamer are highly stable with a well-preserved in-register parallel β-sheet at 330 K, suggesting that the minimal seeds for hIAPP aggregation could be as small as a trimer. The stable parallel in-register C-terminal or N-terminal β-sheet allows the lateral association of multiple hIAPP oligomers or protofilaments to form higher-order protofilaments or fibrils. In contrast, rIAPP oligomers from dimer to pentamer suffer from a significant loss of C-terminal β-sheet and turn conformation. Compared to strong interpeptide interactions stabilizing hIAPP oligomers, the substantial reduction in the level of interpeptide interactions, including hydrogen bonds, contributes to destabilization of the rIAPP oligomers. Additionally, unlike the solvated and disrupted U-turn conformation in rIAPP oligomers, the highly conserved U-turn cavity in the higher-order hIAPP oligomers is dehydrated without accommodating water molecules inside, which help to protect interpeptide association from penetrating water. Structural comparison of hIAPP oligomers with rIAPP oligomers suggests that the disruption of the U-shaped turn conformation appears to be a plausible inhibition pathway to prevent hIAPP aggregation. This work provides a molecular basis for improving our understanding of interactions governing the self-assembly of amyloidogenic hIAPP peptides and nonamyloidogenic rIAPP peptides.

AUTHOR INFORMATION

Corresponding Author

*E-mail: zhengj@uakron.edu. Telephone: (330) 972-2096.

Author Contributions

G.L. and J. Zhao contributed equally to this work.

Funding

G.L. is thankful for financial support from the National Natural Science Foundation of China (Grant 10901169). J. Zheng is thankful for financial support from National Science Foundation CAREER Awards CBET-0952624 and CBET-1158447 and a 3M Non-Tenured Faculty Award.

Notes

The authors declare no competing financial interest.

■ ACKNOWLEDGMENTS

We thank Dr. Robert Tycko for providing the atomic coordinates of the hIAPP fibrillar models. This study utilized (in part) the high-performance Anton cluster at the National Resource for Biomedical Supercomputing.

■ REFERENCES

(1) Khemtémourian, L., Killian, J. A., Höppener, J. W. M., and Engel, M. F. M. (2008) Recent insights in islet amyloid polypeptide-induced membrane disruption and its role in β-cell death in type 2 diabetes mellitus. *Exp. Diabetes Res. 2008*, 421287.

(2) Kapurniotu, A. (2001) Amyloidogenicity and cytotoxicity of islet amyloid polypeptide. *Biopolymers 60*, 438−459.

(3) Cleary, J. P., Walsh, D. M., Hofmeister, J. J., Shankar, G. M., Kuskowski, M. A., Selkoe, D. J., and Ashe, K. H. (2005) Natural oligomers of the amyloid-β protein specifically disrupt cognitive function. *Nat. Neurosci. 8*, 79−84.

(4) Goedert, M. (2001) α-Synuclein and neurodegenerative diseases. *Nat. Rev. Neurosci. 2*, 492−501.

(5) Brender, J. R., Salamekh, S., and Ramamoorthy, A. (2012) Membrane disruption and early events in the aggregation of the diabetes related peptide IAPP from a molecular perspective. *Acc. Chem. Res. 45*, 454−462.

(6) Mirzabekov, T. A., Lin, M.-c., and Kagan, B. L. (1996) Pore formation by the cytotoxic islet amyloid peptide amylin. *J. Biol. Chem. 271*, 1988−1992.

(7) Anguiano, M., Nowak, R. J., and Lansbury, P. T. (2002) Protofibrillar islet amyloid polypeptide permeabilizes synthetic vesicles by a pore-like mechanism that may be relevant to type II diabetes. *Biochemistry 41*, 11338−11343.

(8) Engel, M. F. M., Khemtemourian, L., Kleijer, C. C., Meeldijk, H. J. D., Jacobs, J., Verkleij, A. J., de Kruijff, B., Killian, J. A., and Hoppener, J. W. M. (2008) Membrane damage by human islet amyloid polypeptide through fibril growth at the membrane. *Proc. Natl. Acad. Sci. U.S.A. 105*, 6033−6038.

(9) Brender, J. R., Lee, E. L., Cavitt, M. A., Gafni, A., Steel, D. G., and Ramamoorthy, A. (2008) Amyloid fiber formation and membrane disruption are separate processes localized in two distinct regions of IAPP, the type-2-diabetes-related peptide. *J. Am. Chem. Soc. 130*, 6424−6429.

(10) Meredith, S. C. (2006) Protein denaturation and aggregation. Cellular responses to denatured and aggregated proteins. *Ann. N.Y. Acad. Sci. 1066*, 181−221.

(11) Butterfield, S. M., and Lashuel, H. A. (2010) Amyloidogenic protein-membrane interactions: Mechanistic insight from model systems. *Angew. Chem., Int. Ed. 49* (33), 5628−5654.

(12) Stefani, M. (2010) Biochemical and biophysical features of both oligomer/fibril and cell membrane in amyloid cytotoxicity. *FEBS J. 277*, 4602−4613.

(13) Weise, K., Radovan, D., Gohlke, A., Opitz, N., and Winter, R. (2010) Interaction of hIAPP with model raft membranes and pancreatic β-cells: Cytotoxicity of hIAPP oligomers. *ChemBioChem 11*, 1280−1290.

(14) Last, N. B., Rhoades, E., and Miranker, A. D. (2011) Islet amyloid polypeptide demonstrates a persistent capacity to disrupt membrane integrity. *Proc. Natl. Acad. Sci. U.S.A. 108*, 9460−9465.

(15) Nanga, R. P. R., Brender, J. R., Xu, J., Veglia, G., and Ramamoorthy, A. (2008) Structures of rat and human islet amyloid polypeptide IAPP1-19 in micelles by NMR spectroscopy. *Biochemistry 47*, 12689−12697.

(16) Bedrood, S., Li, Y., Isas, J. M., Hegde, B. G., Baxa, U., Haworth, I. S., and Langen, R. (2012) Fibril structure of human islet amyloid polypeptide. *J. Biol. Chem. 287*, 5235−5241.

(17) Luca, S., Yau, W.-M., Leapman, R., and Tycko, R. (2007) Peptide conformation and supramolecular organization in amylin fibrils: Constraints from solid-state NMR. *Biochemistry 46*, 13505−13522.

(18) Höppener, J. W. M., Jacobs, H. M., Wierup, N., Sotthewes, G., Sprong, M., de Vos, P., Berger, R., Sundler, F., and Ahrén, B. (2008) Human islet amyloid polypeptide transgenic mice: In vivo and ex vivo models for the role of hIAPP in type 2 diabetes mellitus. *Exp. Diabetes Res. 2008*, 697035.

(19) Goldsbury, C., Goldie, K., Pellaud, J., Seelig, J., Frey, P., Muller, S. A., Kistler, J., Cooper, G. J. S., and Aebi, U. (2000) Amyloid fibril formation from full-length and fragments of amylin. *J. Struct. Biol. 130*, 352−362.

(20) Wiltzius, J. J. W., Sievers, S. A., Sawaya, M. R., and Eisenberg, D. (2009) Atomic structures of IAPP (amylin) fusions suggest a mechanism for fibrillation and the role of insulin in the process. *Protein Sci. 18*, 1521−1530.

(21) Makin, S. O., and Serpell, L. C. (2004) Structural characterisation of islet amyloid polypeptide fibrils. *J. Mol. Biol. 335*, 1279−1288.

(22) Wang, L., Middleton, C. T., Singh, S., Reddy, A. S., Woys, A. M., Strasfeld, D. B., Marek, P., Raleigh, D. P., de Pablo, J. J., Zanni, M. T., and Skinner, J. L. (2011) 2DIR spectroscopy of human amylin fibrils reflects stable β-sheet structure. *J. Am. Chem. Soc. 133*, 16062−16071.

(23) Kayed, R., Bernhagen, J., Greenfield, N., Sweimeh, K., Brunner, H., Voelter, W., and Kapurniotu, A. (1999) Conformational transitions of islet amyloid polypeptide (IAPP) in amyloid formation *in vitro*. *J. Mol. Biol. 287*, 781−796.

(24) Soong, R., Brender, J. R., Macdonald, P. M., and Ramamoorthy, A. (2009) Association of highly compact type II diabetes related islet amyloid polypeptide intermediate species at physiological temperature revealed by diffusion NMR spectroscopy. *J. Am. Chem. Soc. 131*, 7079−7085.

(25) Haataja, L., Gurlo, T., Huang, C. J., and Butler, P. C. (2008) Islet Amyloid in Type 2 Diabetes, and the Toxic Oligomer Hypothesis. *Endocr. Rev. 29*, 303−316.

(26) Andrews, M. N., and Winter, R. (2011) Comparing the structural properties of human and rat islet amyloid polypeptide by MD computer simulations. *Biophys. Chem. 156*, 43−50.

(27) Jiang, P., Wei, L., Pervushin, K., and Mu, Y. (2010) pH-Dependent interactions of human islet amyloid polypeptide segments with insulin studied by replica exchange molecular dynamics simulations. *J. Phys. Chem. B 114*, 10176−10183.

(28) Laghaei, R., Mousseau, N., and Wei, G. (2010) Effect of the disulfide bond on the monomeric structure of human amylin studied by combined Hamiltonian and temperature replica exchange molecular dynamics simulations. *J. Phys. Chem. B 114*, 7071−7077.

(29) Laghaei, R., Mousseau, N., and Wei, G. (2011) Structure and thermodynamics of amylin dimer studied by Hamiltonian-temperature replica exchange molecular dynamics simulations. *J. Phys. Chem. B 115*, 3146−3154.

(30) Dupuis, N. F., Wu, C., Shea, J.-E., and Bowers, M. T. (2011) The amyloid formation mechanism in human IAPP: Dimers have β-strand monomer−monomer interfaces. *J. Am. Chem. Soc. 133*, 7240−7243.

(31) Xu, W., Ping, J., Li, W., and Mu, Y. (2009) Assembly dynamics of two-β sheets revealed by molecular dynamics simulations. *J. Chem. Phys. 130*, 164709.

(32) Zhao, J., Yu, X., Liang, G., and Zheng, J. (2011) Structural polymorphism of human islet amyloid polypeptide (hIAPP) oligomers highlights the importance of interfacial residue interactions. *Biomacromolecules 12*, 210−220.

(33) Zhao, J., Yu, X., Liang, G., and Zheng, J. (2011) Heterogeneous triangular structures of human islet amyloid polypeptide (amylin) with internal hydrophobic cavity and external wrapping morphology reveal the polymorphic nature of amyloid fibrils. *Biomacromolecules 12*, 1781−1794.

(34) Murphy, R. D., Conlon, J., Mansoor, T., Luca, S., Vaiana, S. M., and Buchete, N.-V. (2012) Conformational dynamics of human IAPP monomers. *Biophys. Chem. 167*, 1−7.

(35) Reddy, A. S., Wang, L., Singh, S., Ling, Y. L., Buchanan, L., Zanni, M. T., Skinner, J. L., and de Pablo, J. J. (2010) Stable and

metastable states of human amylin in solution. *Biophys. J. 99*, 2208−2216.
(36) Dupuis, N. F., Wu, C., Shea, J.-E., and Bowers, M. T. (2009) Human islet amyloid polypeptide monomers form ordered β-hairpins: A possible direct amyloidogenic precursor. *J. Am. Chem. Soc. 131*, 18283−18292.
(37) Higham, C. E., Jaikaran, E. T. A. S., Fraser, P. E., Gross, M., and Clark, A. (2000) Preparation of synthetic human islet amyloid polypeptide (IAPP) in a stable conformation to enable study of conversion to amyloid-like fibrils. *FEBS Lett. 470*, 55−60.
(38) Padrick, S. B., and Miranker, A. D. (2001) Islet amyloid polypeptide: Identification of long-range contacts and local order on the fibrillogenesis pathway. *J. Mol. Biol. 308*, 783−794.
(39) Yonemoto, I. T., Kroon, G. J. A., Dyson, H. J., Balch, W. E., and Kelly, J. W. (2008) Amylin proprotein processing generates progressively more amyloidogenic peptides that initially sample the helical state. *Biochemistry 47*, 9900−9910.
(40) Williamson, J. A., and Miranker, A. D. (2007) Direct detection of transient α-helical states in islet amyloid polypeptide. *Protein Sci. 16*, 110−117.
(41) Barz, B., and Urbanc, B. (2012) Dimer formation enhances structural differences between amyloid β-protein (1−40) and (1−42): An explicit-solvent molecular dynamics study. *PLoS One 7*, e34345.
(42) Mo, Y., Lu, Y., Wei, G., and Derreumaux, P. (2009) Structural diversity of the soluble trimers of the human amylin(20−29) peptide revealed by molecular dynamics simulations. *J. Chem. Phys. 130*, 125101.
(43) Rivera, E., Straub, J., and Thirumalai, D. (2009) Sequence and crowding effects in the aggregation of a 10-residue fragment derived from islet amyloid polypeptide. *Biophys. J. 96*, 4552−4560.
(44) Yang, Z., Shi, B., Lu, H., Xiu, P., and Zhou, R. (2011) Dewetting transitions in the self-assembly of two amyloidogenic β-sheets and the importance of matching surfaces. *J. Phys. Chem. B 115*, 11137−11144.
(45) Wu, C., Lei, H., and Duan, Y. (2004) Formation of partially ordered oligomers of amyloidogenic hexapeptide (NFGAIL) in aqueous solution observed in molecular dynamics simulations. *Biophys. J. 87*, 3000−3009.
(46) Wu, C., Lei, H., and Duan, Y. (2005) Elongation of ordered peptide aggregate of an amyloidogenic hexapeptide NFGAIL observed in molecular dynamics simulations with explicit solvent. *J. Am. Chem. Soc. 127*, 13530−13537.
(47) Cao, P., Meng, F., Abedini, A., and Raleigh, D. P. (2010) The ability of rodent islet amyloid polypeptide to inhibit amyloid formation by human islet amyloid polypeptide has important implications for the mechanism of amyloid formation and the design of inhibitors. *Biochemistry 49*, 872−881.
(48) Gilead, S., and Gazit, E. (2008) The role of the 14−20 domain of the islet amyloid polypeptide in amyloid formation. *Exp. Diabetes Res. 2008*, 256954.
(49) Middleton, C. T., Marek, P., Cao, P., Chiu, C.-c., Singh, S., Woys, A. M., de Pablo, J. J., Raleigh, D. P., and Zanni, M. T. (2012) Two-dimensional infrared spectroscopy reveals the complex behaviour of an amyloid fibril inhibitor. *Nat. Chem. 4*, 355−360.
(50) Yu, X., Luo, Y., Dinkel, P., Zheng, J., Wei, G., Margittai, M., Nussinov, R., and Ma, B. (2012) Cross-seeding and conformational selection between three- and four-repeat human Tau proteins. *J. Biol. Chem. 287*, 14950−14959.
(51) Ma, B., and Nussinov, R. (2012) Selective molecular recognition in amyloid growth and transmission and cross-species barriers. *J. Mol. Biol. 421*, 172−184.
(52) Dinkel, P. D., Siddiqua, A., Huynh, H., Shah, M., and Margittai, M. (2011) Variations in filament conformation dictate seeding barrier between three- and four-repeat tau. *Biochemistry 50*, 4330−4336.
(53) Andreetto, E., Yan, L.-M., Tatarek-Nossol, M., Velkova, A., Frank, R., and Kapurniotu, A. (2010) Identification of hot regions of the Aβ−IAPP interaction interface as high-affinity binding sites in both cross- and self-association. *Angew. Chem., Int. Ed. 49*, 3081−3085.
(54) Kale, L., Skeel, R., Bhandarkar, M., Brunner, R., Gursoy, A., Krawetz, N., Phillips, J., Shinozaki, A., Varadarajan, K., and Schulten, K. (1999) NAMD2: Greater scalability for parallel molecular dynamics. *J. Comput. Phys. 151*, 283−312.
(55) MacKerell, A. D., Bashford, D., Bellott, M., Dunbrack, R. L., Evanseck, J. D., Field, M. J., Fischer, S., Gao, J., Guo, H., Ha, S., Joseph-McCarthy, D., Kuchnir, L., Kuczera, K., Lau, F. T. K., Mattos, C., Michnick, S., Ngo, T., Nguyen, D. T., Prodhom, B., Reiher, W. E., Roux, B., Schlenkrich, M., Smith, J. C., Stote, R., Straub, J., Watanabe, M., Wiorkiewicz-Kuczera, J., Yin, D., and Karplus, M. (1998) All-atom empirical potential for molecular modeling and dynamics studies of proteins. *J. Phys. Chem. B 102*, 3586−3616.
(56) Miller, Y., Ma, B., and Nussinov, R. (2009) Polymorphism of Alzheimer's Aβ17−42 (p3) oligomers: The importance of the turn location and its conformation. *Biophys. J. 97*, 1168−1177.
(57) Zheng, J., Ma, B., Chang, Y., and Nussinov, R. (2008) Molecular dynamics simulations of Alzheimer's peptide Aβ40 elongation and lateral association. *Front. Biosci. 13*, 3919−3930.
(58) Humphrey, W., Dalke, A., and Schulten, K. (1996) VMD: Visual molecular dynamics. *J. Mol. Graphics 14*, 33−38.
(59) Reddy, A. S., Wang, L., Lin, Y.-S., Ling, Y., Chopra, M., Zanni, M. T., Skinner, J. L., and De Pablo, J. J. (2010) Solution structures of rat amylin peptide: Simulation, theory, and experiment. *Biophys. J. 98*, 443−451.
(60) Reddy, G., Straub, J. E., and Thirumalai, D. (2009) Dynamics of locking of peptides onto growing amyloid fibrils. *Proc. Natl. Acad. Sci. U.S.A. 106*, 11948−11953.
(61) Kajava, A. V., Aebi, U., and Steven, A. C. (2005) The parallel superpleated β-structure as a model for amyloid fibrils of human amylin. *J. Mol. Biol. 348*, 247−252.
(62) Wiltzius, J. J. W., Sievers, S. A., Sawaya, M. R., Cascio, D., Popov, D., Riekel, C., and Eisenberg, D. (2008) Atomic structure of the cross-β spine of islet amyloid polypeptide (amylin). *Protein Sci. 17*, 1467−1474.
(63) Frishman, D., and Argos, P. (1995) Knowledge-based protein secondary structure assignment. *Proteins 23*, 566−579.
(64) Cheon, M., Chang, I., Mohanty, S., Luheshi, L. M., Dobson, C. M., Vendruscolo, M., and Favrin, G. (2007) Structural reorganisation and potential toxicity of oligomeric species formed during the assembly of amyloid fibrils. *PLoS Comput. Biol. 3*, e173.
(65) Thirumalai, D., Reddy, G., and Straub, J. E. (2012) Role of water in protein aggregation and amyloid polymorphism. *Acc. Chem. Res. 45*, 83−92.
(66) Zheng, J., Jang, H., Ma, B., Tsai, C.-J., and Nussinov, R. (2007) Modeling the alzheimer Aβ17−42 fibril architecture: Tight intermolecular sheet-sheet association and intramolecular hydrated cavities. *Biophys. J. 93*, 3046−3057.
(67) Buchete, N.-V., and Hummer, G. (2007) Structure and dynamics of parallel β-sheets, hydrophobic core, and loops in Alzheimer's Aβ fibrils. *Biophys. J. 92*, 3032−3039.
(68) Buchete, N.-V., Tycko, R., and Hummer, G. (2005) Molecular dynamics simulations of Alzheimer's β-amyloid protofilaments. *J. Mol. Biol. 353*, 804−821.
(69) Sawaya, M. R., Sambashivan, S., Nelson, R., Ivanova, M. I., Sievers, S. A., Apostol, M. I., Thompson, M. J., Balbirnie, M., Wiltzius, J. J. W., McFarlane, H. T., Madsen, A. O., Riekel, C., and Eisenberg, D. (2007) Atomic structures of amyloid cross-β spines reveal varied steric zippers. *Nature 447*, 453−457.
(70) Zheng, J., Ma, B., Tsai, C.-J., and Nussinov, R. (2006) Structural stability and dynamics of an amyloid-forming peptide GNNQQNY from the yeast prion sup-35. *Biophys. J. 91*, 824−833.